0.03, to 0.005 as the collision impact parameter, b, is increased from 0.0, 1.0, 2.0, to 3.0 Å. On the basis of the centrifugal potential at the central barrier, the maximum impact parameter for reaction is estimated as 5.2 Å, but the low reaction probability at $b > 2$ Å makes it computationally intractable to sample the complete range of b. Nevertheless, important details of the reaction dynamics are found. The reaction occurs by both direct and indirect mechanisms, with a direct fraction of 0.4, 0.8, 0.8, and ~1.0 for impact parameters of 0.0, 1.0, 2.0, and 3.0 Å, respectively, suggesting the direct reaction dominates at the larger b values. The product energy partitioning for the direct reaction is the same for these four impact parameters, with average fractions of 0.04, 0.23, and 0.73 for rotation, vibration, and translation, respectively. For the indirect trajectories, the average fractions of energy partitioning to rotation (0.28), vibration (0.56), and translation (0.16) are quite different. Because the direct reaction is expected to dominate when trajectories are averaged over all impact parameters, an overall fraction partitioned to translation in the range of 0.6 to 0.7 is expected. This partitioning corresponds to a mean internal excitation of about 0.85 eV, which agrees well with the experimental value of 0.95 eV as given above. The much higher internal excitation for indirect reactions amounts to about 1.9 eV, which is in good agreement with the average energy of the two low-velocity peaks observed in the experiment (Fig. 2D and Fig. 2H, left arrow).

The atomic-level mechanisms for the direct and indirect reactions at 1.9 eV collision energy are substantially different. The direct reaction occurs by the classical S_N2 reaction path, with Cl^- attacking the backside of CH_3I and directly displacing I^- (*8*). The indirect reaction occurs via a roundabout mechanism involving a CH_3 rotation. The principal mode for this mechanism is depicted in Fig. 3, where Cl^- first strikes the side of the CH_3 group, causing it to rotate around the more massive I atom. Then, after one CH_3 revolution, Cl^- attacks the C atom backside and directly displaces I^-. The time between the initial Cl^--CH_3 collision and the departure of I^- ranges around 400 fs. Two variants of the roundabout mechanism, of much lesser importance and with intermediate lifetimes of 1 to 4 ps, were also found. One is identical to the roundabout mechanism, except the departing I^- becomes transiently trapped in the post–reaction potential energy well (Fig. 1). The other is similar to the roundabout mechanism, except CH_3 rotates twice about the I atom. The translational energy partitioning for the roundabout mechanism approximates that of phase space theory (Fig. 2H), which assumes statistical dynamics. This suggests that this mechanism may participate in the statistical product energy partitioning observed for the $Cl^- + CH_3I$ S_N2 reaction at lower collision energies.

This combined experimental and computational study has identified a previously unknown roundabout, CH_3-rotation mechanism for gas-phase S_N2 nucleophilic substitution reactions. This mechanism may also play a role for other S_N2 reactions, such as the $Cl^- + CH_3Br$ reaction, where an energy-dependent change in the reaction mechanism has been discussed (*11*, *29*). It will be of particular interest to determine the role of the roundabout mechanism in other and more complex ion-molecule reactions.

References and Notes

1. See, for example, K. P. C. Vollhardt, N. E. Schore, *Organic Chemistry, Structure and Function* (Pallgrave Macmillan, Basingstoke, UK, 2007).
2. N. Merceron-Saffon, A. Baceiredo, H. Gornitzka, G. Bertrand, *Science* **301**, 1223 (2003).
3. B. Boudaïffa, P. Cloutier, D. Hunting, M. A. Huels, L. Sanche, *Science* **287**, 1658 (2000).
4. M. L. Chabinyc, S. L. Craig, C. K. Regan, J. I. Brauman, *Science* **279**, 1882 (1998).
5. J. K. Laerdahl, E. Uggerud, *Int. J. Mass Spectrom.* **214**, 277 (2002).
6. W. L. Hase, *Science* **266**, 998 (1994).
7. S. Schmatz, *ChemPhysChem* **5**, 600 (2004).
8. W. N. Olmstead, J. I. Brauman, *J. Am. Chem. Soc.* **99**, 4219 (1977).
9. C. H. DePuy, S. Gronert, A. Mullin, V. M. Bierbaum, *J. Am. Chem. Soc.* **112**, 8650 (1990).
10. J.-L. Le Garrec, B. R. Rowe, J. L. Queffelec, J. B. A. Mitchell, D. C. Clary, *J. Chem. Phys.* **107**, 1021 (1997).
11. L. A. Angel, K. M. Ervin, *J. Am. Chem. Soc.* **125**, 1014 (2003).
12. D. S. Tonner, T. B. McMahon, *J. Am. Chem. Soc.* **122**, 8783 (2000).
13. S. T. Graul, M. T. Bowers, *J. Am. Chem. Soc.* **116**, 3875 (1994).
14. A. A. Viggiano, R. A. Morris, J. S. Paschkewitz, J. F. Paulson, *J. Am. Chem. Soc.* **114**, 10477 (1992).
15. S. L. Craig, J. I. Brauman, *Science* **276**, 1536 (1997).
16. S. L. VanOrden, R. M. Pope, S. W. Buckner, *Org. Mass Spectrom.* **26**, 1003 (1991).
17. R. Wester, A. E. Bragg, A. V. Davis, D. M. Neumark, *J. Chem. Phys.* **119**, 10032 (2003).
18. L. Sun, K. Song, W. L. Hase, *Science* **296**, 875 (2002).
19. C. Hennig, S. Schmatz, *J. Chem. Phys.* **122**, 234307 (2005).
20. D. C. Clary, *Science* **279**, 1879 (1998).
21. P. Ayotte, J. Kim, J. A. Kelley, S. B. Nielsen, M. A. Johnson, *J. Am. Chem. Soc.* **121**, 6950 (1999).
22. J. Mikosch *et al.*, *Phys. Chem. Chem. Phys.* **8**, 2990 (2006).
23. J. J. Lin, J. Zhou, W. Shiu, K. Liu, *Science* **300**, 966 (2003).
24. Special care is taken to suppress formation of clusters in the supersonic expansion, as identified by photodissociation with ultraviolet (UV) laser light. Extraction fields are multistage to enable velocity mapping and spatial focusing of product ions spread over a large volume. The velocity distribution of the anion reactant beam is measured before and after recording each of the product velocity images. The velocity distribution of the neutral beam is measured by ionization with a pulsed electron beam and subsequent velocity map imaging. The beam spreads represent the largest contribution to the experimental resolution, such that effects of imperfect velocity mapping and slicing can be neglected. A few product anions are formed per bunch crossing; the repetition rate of the experiment is 10 Hz. We accounted for the decreased signal of fast product ions by using a one-dimensional, experimentally determined efficiency function.
25. W. J. Chesnavich, M. T. Bowers, *J. Chem. Phys.* **66**, 2306 (1977).
26. The aug-cc-pVDZ basis set was used for the C, H, and Cl atoms. For iodine, the Wadt and Hay effective core potential (ECP) was used for the core electrons and an uncontracted 3s,3p basis set for the valence electrons (*30*). This iodine basis was augmented by a d-polarization function with a 0.262 exponent and s, p, and d diffuse functions with exponents of 0.034, 0.039, and 0.0873, respectively (*31*). This basis is denoted as ECP/aug-cc-pVDZ in the text.
27. U. Lourderaj, K. Song, T. L. Windus, Y. Zhuang, W. L. Hase, *J. Chem. Phys.* **126**, 044105 (2007).
28. M. N. Glukhovtsev, A. Pross, L. Radom, *J. Am. Chem. Soc.* **118**, 6273 (1996).
29. Y. Wang, W. L. Hase, H. Wang, *J. Chem. Phys.* **118**, 2688 (2003).
30. W. R. Wadt, P. J. Hay, *J. Chem. Phys.* **82**, 284 (1985).
31. W.-P. Hu, D. G. Truhlar, *J. Phys. Chem.* **98**, 1049 (1994).

32. This work is supported by the Deutsche Forschungsgemeinschaft under contract no. WE 2661/4-1 and by the Eliteförderprogramm der Landesstiftung Baden-Württemberg. We thank U. Frühling and D. Schwalm for their support in setting up the experiment. The contribution from TTU is based on work supported by the NSF under grant no. CHE-0615321 and the Robert A. Welch Foundation under grant no. D-0005. Support was also provided by the TTU High-Performance Computing Center.

7 September 2007; accepted 12 November 2007
10.1126/science.1150238

Tidal Modulation of Nonvolcanic Tremor

Justin L. Rubinstein,[1]* Mario La Rocca,[2] John E. Vidale,[1] Kenneth C. Creager,[1] Aaron G. Wech[1]

Episodes of nonvolcanic tremor and accompanying slow slip recently have been observed in the subduction zones of Japan and Cascadia. In Cascadia, such episodes typically last a few weeks and differ from "normal" earthquakes in their source location and moment-duration scaling. The three most recent episodes in the Puget Sound/southern Vancouver Island portion of the Cascadia subduction zone were exceptionally well recorded. In each episode, we saw clear pulsing of tremor activity with periods of 12.4 and 24 to 25 hours, the same as the principal lunar and lunisolar tides. This indicates that the small stresses associated with the solid-earth and ocean tides influence the genesis of tremor much more effectively than they do the genesis of normal earthquakes. Because the lithostatic stresses are 10^5 times larger than those associated with the tides, we argue that tremor occurs on very weak faults.

Shortly after the discovery of both nonvolcanic tremor (*1*) and recurring slow-slip events (*2*, *3*), Rogers and Dragert determined that these two phenomena occur coincident with each other at regular intervals in the Cascadia subduction zone (*4*). They termed this phenomenon episodic tremor and slip (ETS). Soon thereafter, ETS was also observed in the Nankai Trough in Japan (*5*). ETS falls into a newly identified class of geophysical phenomena that are distinct from "normal" earthquakes. For these slow-slip phenomena, seismic moment scales with event duration (*6*), whereas for earthquakes, moment scales with the cube of event

duration (*7*). The relative locations of nonvolcanic tremor and earthquakes also indicate that they are different processes. In Cascadia, tremor appears to fill volumes of crust that have little or no seismicity (*8*), whereas on the San Andreas Fault, tremor is found below crustal seismicity (*9*). Precise locations of low-frequency earthquakes in Japan, which have been shown to make up a substantial part of nonvolcanic tremor (*10*), place them well above the only nearby seismicity (*11*).

ETS has been interpreted by many as intermittent accelerated slip located between the locked and freely slipping portions of subduction megathrust faults, possibly mediated by pressure fluctuations of fluids rising from the subducting slab (*4–6*, *10*, *11*). However, a wide range of other physical mechanisms for ETS remains on the table. Here we spotlight a striking difference from normal earthquakes: The amplitude of tremor strongly correlates with tidal stresses. Many have sought a correlation between earthquakes and the stress fluctuations induced by the tides, but only those examining the most favorable conditions for triggering (*12–17*) see any correlation of earthquakes with the tides. Careful studies of large earthquake data sets find no such correlation (*18–21*).

The ETS episodes in the portion of the Cascadia subduction zone near Puget Sound and southern Vancouver Island have a periodicity of approximately 14 months, with each episode lasting 2 to 3 weeks. The last three major ETS episodes in this region were in July 2004, September 2005, and January 2007. Although each event had its own characteristics, they all covered approximately the same region from southern Puget Sound to southern Vancouver Island (Fig. 1). Before each of these events, we deployed focused seismic arrays to better locate and characterize ETS. Each array recorded one ETS event. The arrays had 5 to 11 stations and their apertures ranged from 0.6 to 2.0 km. In this study, we used five of these arrays (Fig. 1) to filter out noise and to closely examine how the amplitude of tremor varies with time (*22*). This allowed us investigate whether nonvolcanic tremor has a tidal periodicity. Two additional arrays that were deployed (LO in 2004 and BD in 2007) and two individual stations (SE-1 and PA-15) were not used because they were dominated by cultural noise.

The amplitude of the tremor varied over time and from array to array (Fig. 2). The recorded amplitude of the tremor depended on both the strength of the tremor and the proximity of the array to the migrating tremor source. For example, it is evident that the 2007 ETS episode migrated from the south to the north, because early in the ETS event, the amplitudes were larger at the southern array PL than at array BS. A few days later, amplitudes were largest at array BS (Fig. 2C).

When examining the amplitude of the tremor for the 2004 and 2007 ETS episodes, one can clearly identify a twice-a-day pulsing of tremor activity, and there are suggestions of such a periodicity in the 2005 episode (Fig. 2 and fig. S1). Once-a-day periods are also visible in several of the time series. The likely signals from tidal stresses would be roughly once- and twice-a-day signals from the gravitational influence of the Sun and Moon. As with all seismic data, we also have to contend with cultural noise that has a daily cycle and often a week/weekend cycle. These signals are visible, for example, in the nontremor interval at the PA array (Fig. 2).

To present a more quantitative evaluation of the periodicity of the tremor, we took a 13-day window of the tremor and computed its spectrum (*22*). The approximately twice-daily periodicity visible in the amplitude time series for each array (Fig. 2) is even more clear when we examine the spectra during ETS episodes (Fig. 3). At all five arrays, there is a strong peak in the spectral amplitude at 12.4 hours, the period of the principal lunar tide. This is in contrast with the characterization of the noise at these same arrays, many of which have a much weaker peak at periods of approximately 12 hours. The strongest tidal forcing is at a period of 12.4 hours, so, given its presence in all three ETS episodes, its absence at other times, and the lack of alternative sources, we can confidently identify the 12.4-hour peaks as due to tidal stresses. The strong 12.4-hour periodicity of the tremor amplitudes is evident when one compares the tremor amplitudes to a sinusoid with 12.4-hour periodicity (fig. S1). Many peaks in the tremor amplitude line up with peaks in an aligned 12.4-hour–period sinusoid.

To quantify the influence of the 12.4-hour lunar tide on the tremor, we examined the relationship between tremor amplitude and its phasing in a best-fit 12.4-hour periodic model (Fig. 4). To do this, we converted time into a phase angle, given a function with a 12.4-hour periodicity. This means that we can now express tremor amplitude as a function of phase instead of time. For each degree of phase, we computed the mean amplitude of the tremor over all ~25 times that particular phase angle repeated in the 13-day window. We then stacked these curves for all five arrays deployed to get an overall sense of how the tides influenced the amplitude of tremor. Using this calculation, we find that tremor amplitude varies smoothly as a function of phase in a sinusoidal fashion. Tremor amplitude varies strongly with phase; the variance of the amplitude is 33.4% from the mean. This is in strong contrast with the results from same methodology applied to the noise. The noise shows no significant amplitude variation with phase, having a variance of 3.3% from the mean.

During the ETS episodes, we also identified a strong peak in the spectra at a range of periods from 24 to 25 hours, the period of the lunisolar and lunar declination tides (Fig. 3). This peak is more difficult to interpret than those at 12.4 hours, because this is the period at which we would expect to identify cultural noise. In fact, we expect that the rather strong source at a period of 24 hours during periods without ETS is a result of cultural noise (Fig. 3C). Fortunately, we have no reason to believe that the cultural

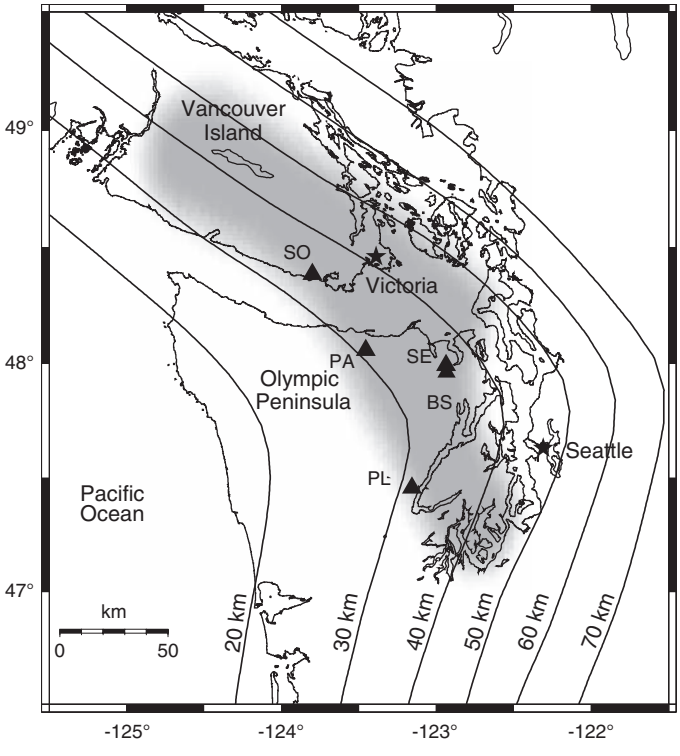

Fig. 1. Map of the study region. Seismic arrays used to record tremor (triangles), the approximate source region of Puget Sound/southern Vancouver Island ETS episodes (shaded region), and isodepths of the plate interface between the Juan de Fuca and North American plates (lines) are indicated on the map.

[1]Department of Earth and Space Science, University of Washington, Box 351310, Seattle, WA 98195, USA. [2]Istituto Nazionale di Geofisica e Vulcanologia–Osservatorio Vesuviano, Via Diocleziano, 328-80124 Napoli, Italy.

*To whom correspondence should be addressed. E-mail: justin@ess.washington.edu

noise that we observe at our sites should be variable from any one period of time to another. Therefore, the much larger spectral amplitudes at periods of 24 to 25 hours during ETS than when ETS is not occurring indicate that tremor is being strongly forced at a daily periodicity in addition to the twice-daily periodicity discussed earlier. We also note that the peaks in tremor amplitude that have an ~24-hour periodicity do not correlate with daylight hours, when cultural noise is at a maximum. This lends further support to our argument that the 24-hour periodicity of the tremor is real. Because of the complication of having two sources of energy that are periodic at 24 hours and do not have the same phasing, we elected not to examine the relationship between amplitude and phase at these periods, because the noise and tremor would interfere with each other.

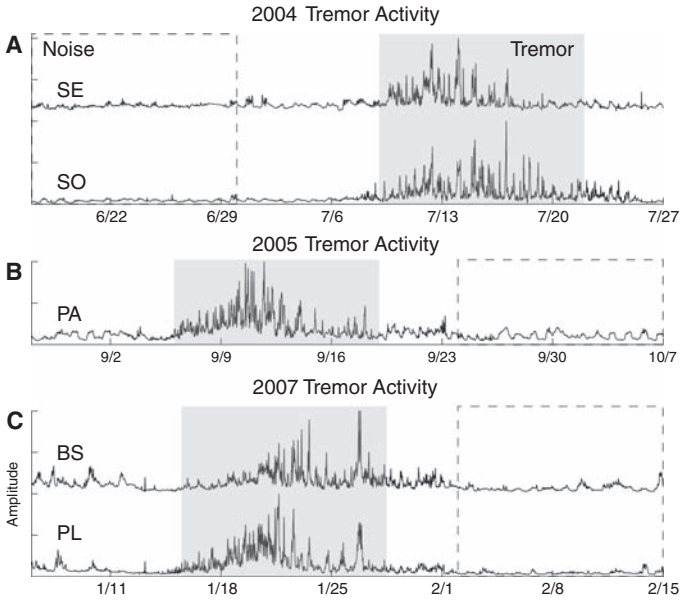

Fig. 2. Tremor amplitudes for ETS episodes in 2004 (**A**), 2005 (**B**), and 2007 (**C**). Each line represents the amplitude of a stack of envelope amplitudes for a single array, each of which recorded a single ETS episode. These stacks were low-pass filtered at a period of 1 hour to distill signals at the frequencies we are interested in. Earthquakes and glitches were removed before stacking. Before computing the envelope, seismograms were band-pass filtered between 1 and 8 Hz. The shaded regions represent a 13-day period during each ETS episode when tremor was strongest at the arrays we were using. The ETS episodes for these events lasted longer than the 13-day windows highlighted; we focused on the periods when recordings of tremor were strongest, when the ETS sources were passing near the arrays. These shaded regions are the regions used to analyze the periodicity of tremor. The dashed-boxed regions represent a 13-day window in which there was no substantial tremor and were used to characterize the noise. Amplitude was normalized at each array by maximum amplitude.

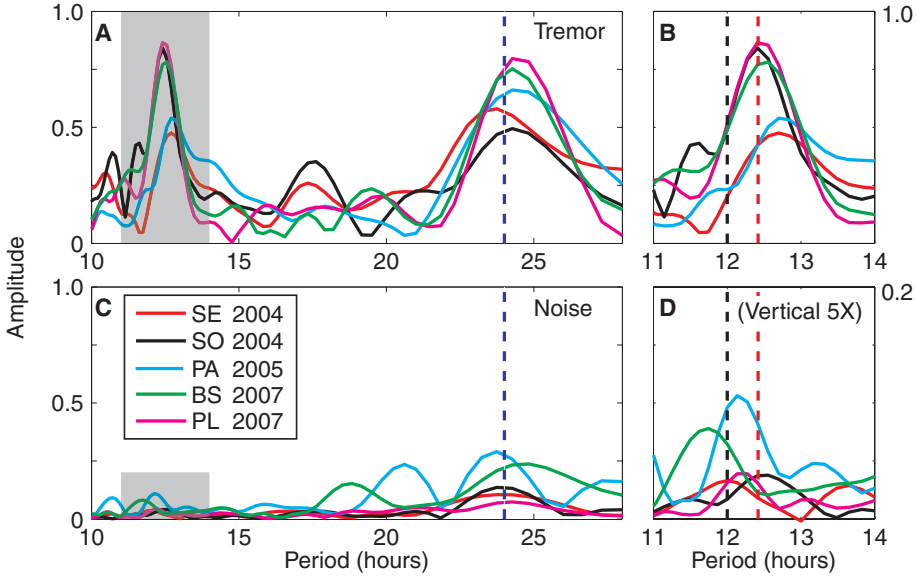

Fig. 3. Spectra of the 13-day windows of tremor (**A** and **B**) and noise (**C** and **D**). Shaded regions in (A) and (C) represent the region that is shown in a zoom in (B) and (D). (D) has been rescaled by a factor of 5. Amplitudes in each panel have been normalized so that the area under each curve in (A) is equal. The variation in amplitudes of the noise [(C) and (D)] indicates the variation in the signal-to-noise ratios at individual arrays; that is, arrays with higher amplitudes of noise have lower signal-to-noise ratios. Dashed vertical lines indicate the strong tidal periods of 12, 12.4, and 24 hours.

We have conducted exploratory modeling of the ocean tidal stresses, finding peak-to-peak values of 15 KPa on the Cascadia subduction interface at depth. Solid-earth tides are also likely to be important, inducing stresses on the order of 5 KPa (*13*). A direct correlation of tremor with the phase of stressing proved beyond the scope of this study. Such correlation would require tidal stress calculations that account for the complexities of tremor as a moving source (*4*), variability in the orientation and even polarity of tidal stresses across the source region, and variability with depth for the appropriate loading geometry. We did compare tremor amplitude and tidal heights (fig. S2), because the normal stress effect of water loading is simple: An increment in water increases normal stress with a diminishing effect with depth. We found that tremor is stronger at periods of high water and therefore periods of increased normal stress. This is in line with the findings of Shelly *et al.* (*23*), who argue that the increment in water height above the subducting slab will slightly decouple the subduction zone and thus allow for increased tremor. An alternate explanation is to consider that the increase in water height above the overriding plate (and the tremor) is increasing friction on the already slipping subduction zone, causing the slow-slip event to radiate more energy. There are undoubtedly other viable explanations for this correlation, but they require knowledge of the shear stresses associated with ocean loading or the earth tides, which will both have a constant phase relative to the ocean tides and the tremor.

Other recent studies have shown twice-daily tidal periodicities in ETS tremor in Japan (*23*, *24*). To explain the propensity for tremor at certain periods of time, they suggest that solid-earth tides (*24*) and ocean tides (*23*) increase the Coulomb failure stress on the plate interface. We do not yet know whether the Coulomb model can explain our observations.

We have shown that tidal modulation at both daily and twice-daily frequencies is a pervasive feature of all three recent episodes in the best-instrumented tremor source region in Cascadia. The stresses associated with these tides are on the order of 15 KPa, approximately 10^5 times smaller than the lithostatic stresses at the depth where tremor radiates. Although it seems improbable that such small stress changes would have such a dramatic effect, there is supporting evidence that small stress changes can influence the genesis of nonvolcanic tremor. A recent study (*25*) has shown that nonvolcanic tremor was triggered in Cascadia by the surface waves of the moment magnitude 7.8 Denali earthquake, which imparted shear stress changes of ~40 Kpa. Similar observations of teleseismic earthquakes triggering tremor have also been made in California (*26*) and Japan (*27*–*29*).

Our observation that tremor is strongly modulated by the tides shows that the physical pro-

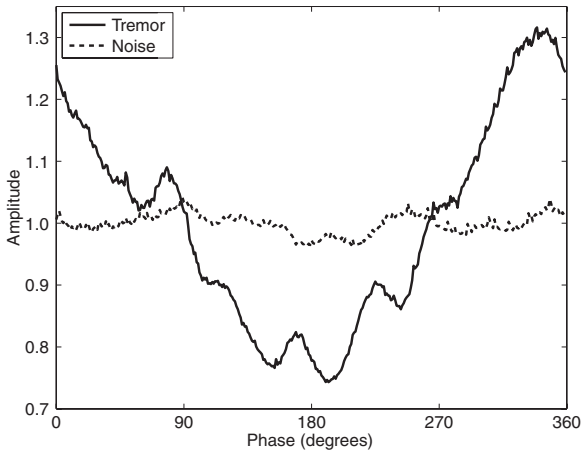

Fig. 4. Amplitude versus phase for a 12.4-hour tidal cycle. In this figure, we compare the variation of the amplitude of tremor during the 13-day ETS windows (solid line) and the 13-day noise windows (dotted line) according to phase in the best-fitting 12.4-hour–period tidal cycle. Phase for each array was determined by cross-correlating a 12.4-hour–period cosine function with the tremor and noise amplitude functions. The amplitude for each degree at each array was averaged over the 25 to 26 times that phase occurred in the 13-day window examined. The amplitudes at the five arrays were averaged for both noise and tremor and were then normalized so that the mean of each curve is 1.

cesses underpinning nonvolcanic tremor are substantially different from those governing earthquakes, which are not typically affected by the tides. ETS appears to represent slow ongoing failure, and thus any increment in stress should affect the failure rate, regardless of the stress state. We believe that this failure is occurring on very weak faults, because small stresses will have a much larger effect on a low-stress fault than a high-stress one. These faults could be very low-friction or, similarly, occur in the presence of near-lithostatic pore pressures.

References and Notes

1. K. Obara, *Science* **296**, 1679 (2002).
2. H. Dragert, K. L. Wang, T. S. James, *Science* **292**, 1525 (2001).
3. M. M. Miller, T. Melbourne, D. J. Johnson, W. Q. Sumner, *Science* **295**, 2423 (2002).
4. G. Rogers, H. Dragert, *Science* **300**, 1942 (2003).
5. K. Obara, H. Hirose, F. Yamamizu, K. Kasahara, *Geophys. Res. Lett.* **31**, L23602 (2004).
6. S. Ide, G. C. Beroza, D. R. Shelly, T. Uchide, *Nature* **447**, 76 (2007).
7. H. Houston, *J. Geophys. Res.* **106**, 11137 (2001).
8. H. Kao *et al.*, *Nature* **436**, 841 (2005).
9. R. M. Nadeau, D. Dolenc, *Science* **307**, 389 (2005).
10. D. R. Shelly, G. C. Beroza, S. Ide, *Nature* **446**, 305 (2007).
11. D. R. Shelly, G. C. Beroza, S. Ide, S. Nakamula, *Nature* **442**, 188 (2006).
12. D. Emter, in *Tidal Phenomena, Lecture Notes in Earth Sciences*, H. Wilhelm, W. Zurn, H.-G. Wenzel, Eds. (Springer-Verlag, Berlin, 1997), vol. 66, pp. 293–309.
13. E. S. Cochran, J. E. Vidale, S. Tanaka, *Science* **306**, 1164 (2004).
14. S. R. McNutt, R. J. Bevan, *Nature* **294**, 615 (1981).
15. W. S. D. Wilcock, *Geophys. Res. Lett.* **28**, 3999 (2001).
16. M. Tolstoy, F. L. Vernon, J. A. Orcutt, F. K. Wyatt, *Geology* **30**, 503 (2002).
17. D. F. Stroup, D. R. Bohnenstiehl, M. Tolstoy, F. Waldhauser, R. T. Weekly, *Geophys. Res. Lett.* **34**, L15301 (2007).
18. M. McNutt, T. H. Heaton, *Calif. Geol.* **34**, 12 (1981).
19. E. S. Cochran, J. E. Vidale, *Geophys. Res. Lett.* **34**, L04302 (2007).
20. J. E. Vidale, D. C. Agnew, M. J. S. Johnston, D. H. Oppenheimer, *J. Geophys. Res.* **103**, 24567 (1998).
21. M. Kennedy, J. E. Vidale, M. Parker, *Seismol. Res. Lett.* **75**, 607 (2004).
22. Materials and methods are available as supporting material on *Science* Online.
23. D. R. Shelly, G. C. Beroza, S. Ide, *Geochem. Geophys. Geosyst.* **8**, Q10014 (2007).
24. R. Nakata, N. Suda, H. Tsuruoka, *Eos* **87**, Fall Meet. Suppl., Abstract V41A-1700.
25. J. L. Rubinstein *et al.*, *Nature* **448**, 579 (2007).
26. J. Gomberg *et al.*, *Science* **319**, 173 (2008).
27. M. Miyazawa, E. E. Brodsky, paper presented at the Seismological Society of Japan 2007 Fall Meeting, Sendai, Japan, 25 October 2007.
28. M. Miyazawa, J. Mori, *Geophys. Res. Lett.* **32**, L10307 (2005).
29. M. Miyazawa, J. Mori, *Geophys. Res. Lett.* **33**, L05303 (2006).
30. C. W. Ulberg, thesis, Carleton College, Northfield, MN (2007).

31. A summer undergraduate project (*30*) paved the road for parts of this study. Incorporated Research Institutions for Seismology, Earthscope, and Istituto Nazionale di Geofisica e Vulcanologia provided instruments for the various deployments. D. Agnew provided invaluable help and insight into the tides. J. Sweet assisted with the mapping of the tremor episodes. J. Gomberg, S. Malone, H. Houston, and two anonymous reviewers provided comments that improved this manuscript.

Supporting Online Material

www.sciencemag.org/cgi/content/full/1150558/DC1
Materials and Methods
Figs. S1 and S2

17 September 2007; accepted 13 November 2007
Published online 22 November 2007;
10.1126/science.1150558
Include this information when citing this paper.

Isotopic Evidence for Glaciation During the Cretaceous Supergreenhouse

André Bornemann,[1,2]* Richard D. Norris,[1] Oliver Friedrich,[1,3] Britta Beckmann,[4] Stefan Schouten,[5] Jaap S. Sinninghe Damsté,[5] Jennifer Vogel,[1] Peter Hofmann,[4] Thomas Wagner[6]

The Turonian (93.5 to 89.3 million years ago) was one of the warmest periods of the Phanerozoic eon, with tropical sea surface temperatures over 35°C. High-amplitude sea-level changes and positive $\delta^{18}O$ excursions in marine limestones suggest that glaciation events may have punctuated this episode of extreme warmth. New $\delta^{18}O$ data from the tropical Atlantic show synchronous shifts ~91.2 million years ago for both the surface and deep ocean that are consistent with an approximately 200,000-year period of glaciation, with ice sheets of about half the size of the modern Antarctic ice cap. Even the prevailing supergreenhouse climate was not a barrier to the formation of large ice sheets, calling into question the common assumption that the poles were always ice-free during past periods of intense global warming.

Despite the extreme warmth of the Turonian (*1*–*3*) [93.5 to 89.3 million years ago (Ma) (*4*)], it has been argued that there may have been several stages of continental ice growth during the period, reflected in both erosional surfaces and geochemical records associated with possible glaciation-induced sea-level falls (*5*–*7*). Rapid decreases (<1 million years) in sea level are known from diverse locations in the Turonian of northern Europe, North America, and the Russian Platform and are estimated at magnitudes of 25 to 40 m (*7*, *8*) or even more (*9*). These rapid changes in sea level are too fast and too widespread to be accounted for by tectonic processes and were therefore plausibly triggered by glacioeustasy (*7*, *10*). Further evidence comes from positive $\delta^{18}O$ excursions in marine, but diagenetically altered, limestone sequences (*5*, *11*) and brachiopod isotope data (*6*). However, evidence from sedimentological findings such as ice-rafted debris is still lacking, and unequivocal $\delta^{18}O$ records of well-preserved open-ocean foraminifera are rare, are of low resolution, or do not support the idea of Late Cretaceous ice sheets (*12*). Moreover, there is only a poor understanding of how large ice sheets might grow in a period when tropical sea surface temperatures (SSTs) exceed 35°C (*3*, *13*) and high-latitude temperatures are in excess of 20°C (*2*, *14*).

We used two independent techniques to estimate SSTs during the early Late Cretaceous. One proxy is the $\delta^{18}O$ paleothermometer, which we applied to monospecific planktic foraminiferal samples from a 40-m-thick, organic carbon–rich, laminated marlstone succession of Turonian to Santonian age from the western equatorial Atlantic at Demerara Rise [Ocean Drilling Program (ODP) Site 1259]. These sediments contain planktic foraminifera with a "glassy" appearance and pristine, well-preserved wall textures (*15*).